ADVANCES IN ATMOSPHERIC SCIENCES, VOL. 31, JULY 2014, 836–850

CMIP5/AMIP GCM Simulations of East Asian Summer Monsoon

FENG Jinming*[1,2], WEI Ting[3], DONG Wenjie[3], WU Qizhong[2], and WANG Yongli[1]

[1]*Key Laboratory of Regional Climate-Environment Research for Temperate East Asia, Institute of Atmospheric Physics, Chinese Academy of Sciences, Beijing* 100029

[2]*College of Global Change and Earth System Science, Beijing Normal University, Beijing* 100875

[3]*State Key Laboratory of Earth Surface Processes and Resource Ecology, Beijing Normal University, Beijing* 100875

(Received 25 July 2013; revised 4 November 2013; accepted 5 December 2013)

ABSTRACT

The East Asian summer monsoon (EASM) is a distinctive component of the Asian climate system and critically influences the economy and society of the region. To understand the ability of AGCMs in capturing the major features of EASM, 10 models that participated in Coupled Model Intercomparison Project/Atmospheric Model Intercomparison Project (CMIP5/AMIP), which used observational SST and sea ice to drive AGCMs during the period 1979–2008, were evaluated by comparing with observations and AMIP II simulations. The results indicated that the multi-model ensemble (MME) of CMIP5/AMIP captures the main characteristics of precipitation and monsoon circulation, and shows the best skill in EASM simulation, better than the AMIP II MME. As for the Meiyu/Changma/Baiyu rainbelt, the intensity of rainfall is underestimated in all the models. The biases are caused by a weak western Pacific subtropical high (WPSH) and accompanying eastward southwesterly winds in group I models, and by a too strong and west-extended WPSH as well as westerly winds in group II models. Considerable systematic errors exist in the simulated seasonal migration of rainfall, and the notable northward jumps and rainfall persistence remain a challenge for all the models. However, the CMIP5/AMIP MME is skillful in simulating the western North Pacific monsoon index (WNPMI).

Key words: CMIP5/AMIP, AMIP II, East Asian summer monsoon, multi-model ensemble

Citation: Feng, J. M., T. Wei, W. J. Dong, Q. Z. Wu, and Y. L. Wang, 2014: CMIP5/AMIP GCM Simulations of East Asian Summer Monsoon. *Adv. Atmos. Sci.*, **31**(4), 836–850, doi: 10.1007/s00376-013-3131-y.

1. Introduction

The East Asian summer monsoon (EASM) is a distinctive component of the Asian climate system, and characterized by wind reversal and heavy precipitation during summer over East Asia (EA) (Lau and Li, 1984). The evolution and variability of the monsoon have a big impact on human society across the region. Therefore, better prediction of the monsoon's variation may greatly benefit those people inhabiting the region. As part of that aim, atmospheric general circulation models (AGCMs) have been developed and applied widely in monsoon diagnostics and prediction studies (Shukla and Fennessy, 1994; Liang et al., 1995; Webster et al., 1998; Meehl et al., 2006; Kim et al., 2008).

The Atmospheric Model Intercomparison Project (AMIP) is a series of coordinated international efforts to perform global climate simulations using AGCMs. All the simulations of AMIP employ the same SST, sea ice, solar constant, and CO_2 concentration, thus enabling intercomparison among the GCMs that have been integrated under standard conditions. The AMIP-type simulations are routinely performed at many climate centers in order to evaluate atmospheric model performance. Among these simulations, the predictability and variability of monsoon covering the period 1950–2000 is an active area of research (Kucharski et al., 2009; Zhou et al., 2009b), and many such studies have been carried out and published using AMIP I and AMIP II data (Sperber and Palmer, 1996; Ferranti et al., 1997; Gadgil and Sajani, 1998; Liang et al., 2001; Kang et al., 2002; Lin and Wang, 2002; Wang et al., 2004; Wang et al., 2005; Wu and Kirtman, 2007; Kim et al., 2008; Zhou et al., 2009a; Zhou and Zhang, 2011).

The latest systematic intercomparison of state-of-the-art atmospheric model components is currently being coordinated under phase five of the Coupled Model Intercomparison Project (CMIP5), including AMIP simulations. This new project will most notably provide a multi-model context for examining the predictability of EASM and exploring the response of many state-of-the-art AGCMs to observed variations in SST and sea ice during 1979–2008, related to the latest global warming (Taylor et al., 2012, 2013). Therefore, it is very important to evaluate the ability of these models to reproduce the variation of EASM on seasonal to interan-

* Corresponding author: FENG Jinming
Email: fengjm@tea.ac.cn

nual scales when forced by observed variation in SST and sea ice. It is also expected that the simulations from CMIP5 will provide a clear picture of the future development needs of AGCMs.

In this study, the ability of current AGCMs in modeling the climatological variations of EASM and regional rainbelts is examined. In the intercomparison, the simulations of individual models are analyzed. We emphasize the performance of the models as a whole and seek to summarize the systematic errors that are common to a group of AGCMs in simulating the climatological variation of the EASM. Furthermore, ensemble simulations from 11 AGCMs that participated in AMIPII are shown to compare with the CMIP5/AMIP simulations thus helping us to understand the improvements needed for the models.

The paper is organized as follows. A description of the CMIP5/AMIP and AMIP II models and data is provided in section 2 Climatic mean states of EASM are presented in section 3, followed by seasonal migration of the EASM rainbelt in section 4 Section 5 reports the interannual variation of EASM, followed by the overall conclusions of the study in the final section.

2. The CMIP5/AMIP and AMIP II models and data

The climate modeling experiments analyzed here are the archived CMIP5/AMIP and AMIPII simulations of atmosphere–land–only models. These models are forced by the observed monthly global sea ice and SST data from the Hadley Centre for Climate Prediction for the period January 1979 to December 2008 (for simulations of AMIP II the period is 1979–99). Table 1 summarizes the models used in the study. Most of the CMIP5/AMIP models used here are the new versions of AMIP II models with finer spatial resolution. In the CMIP5/AMIP group, the highest atmospheric resolution is 0.5° (lat) ×0.625° (lon) (GFDL-HIRAM-C180 and GISS-E2-R). Most models have a resolution about 1°–2° or are approximately 100–200 km in grid size. The basic information for the models is given in Table 1 and further detailed description of the models and experimental designs are available online at http://cmip-pcmdi.llnl.gov/cmip5. For each model, the analysis was performed with daily precipitation as well as monthly precipitation, winds and geopotential height data. All datasets for the models were re-gridded to be consistent with observations before analysis.

The National Center for Atmospheric Research/Department of Energy (NCEP/DOE) Reanalysis II data (hereafter, NCEP2; Kanamitsu et al., 2002) and Global Precipitation Climatology Project precipitation data (GPCP; Adler et al., 2003) were used to validate the models. The spatial resolution of these data is 2.5° × 2.5°.

3. Climatic mean states

3.1. *Precipitation*

The EASM domain covers the region (20°–45°N, 110°–140°E), encompassing eastern China, Japan, Korea and the adjacent seas (Wang and Lin, 2002). There are two rainbelts in EA during boreal summer (June–August) based on observation (Fig. 1). One extends from East China to the northwestern Pacific, which is known as the subtropical Meiyu/Changma/Baiyu rainbelt. The other is over the tropical western Pacific. A relatively dry region, covered by the western Pacific subtropical high (WPSH), emerges between the two rainbelts. As shown in Fig. 1, GFDL-HIRAM-C180, GISS-E2-R, HadGEM2-A, INM-CM4, MIROC5 and MRI-CGCM3 simulate a stronger tropical rainbelt; while BNU-ESM, CNRM-CM5, MPI-ESM-LR and NorESM1-M show a weaker simulation of the major rainbelt over the tropics. Note that this rainbelt is well reproduced by the multi-model ensemble mean (MME) of CMIP5/AMIP models. However,

Table 1. Climate models whose AMIP simulations were analyzed in this study.

Model name		Center/country	Resolution (lat.×lon.)		Reference
CMIP5	AMIPII		CMIP5	AMIPII	
CNRM-CM5	CNRM-CM3	CNRM/France	2.8° × 2.8°	2.8° × 2.8°	Voldoire et al. (2011)
GFDL-HIRAM-C180	GFDL-CM2.1	NOAA/United States	1.4° × 1.4°	2.0° × 2.5°	Zhao et al. (2009)
GISS-E2-R	GISS	NASA/United States	0.5° × 0.625°	4° × 5°	Schmidt et al. (2006)
HadGEM2-A	HadGEM1	Met Office/United Kingdom	0.5° × 0.625°	1.25° × 1.875°	Collins et al. (2008)
INM-CM4	INM-CM3	INM/Russia	1.25° × 1.875°	4° × 5°	Volodin et al. (2010)
MIROC5	MIROC3.2-hires	University of Tokyo/ NIES/MEST/Japan	1.5° × 2.0°	1.125° × 1.125°	Watanabe et al. (2010)
	MIROC3.2-medres			2.8° × 2.8°	
MRI-CGCM3	MRI–CGCM2	MRI/Japan	1.4° × 1.4°	2.8° × 2.8°	Yukimoto et al. (2011)
MPI-ESM-LR	ECHAM5	MPI/Germany	1.875° × 1.875°	1.875° × 1.875°	Roeckner et al. (2003)
NorESM1-M		NCC/Norway	1.125° × 1.56°		Bentsen et al. (2012)
BNU-ESM		BNU/China	1.875° × 2.5°		Wu et al. (2013)
	FGOALS1.0-g	IAP/China		3.0° × 2.8°	Yu et al. (2004)
	CCSM3	NCAR/ United States		1.4° × 1.4°	Collins et al. (2006)

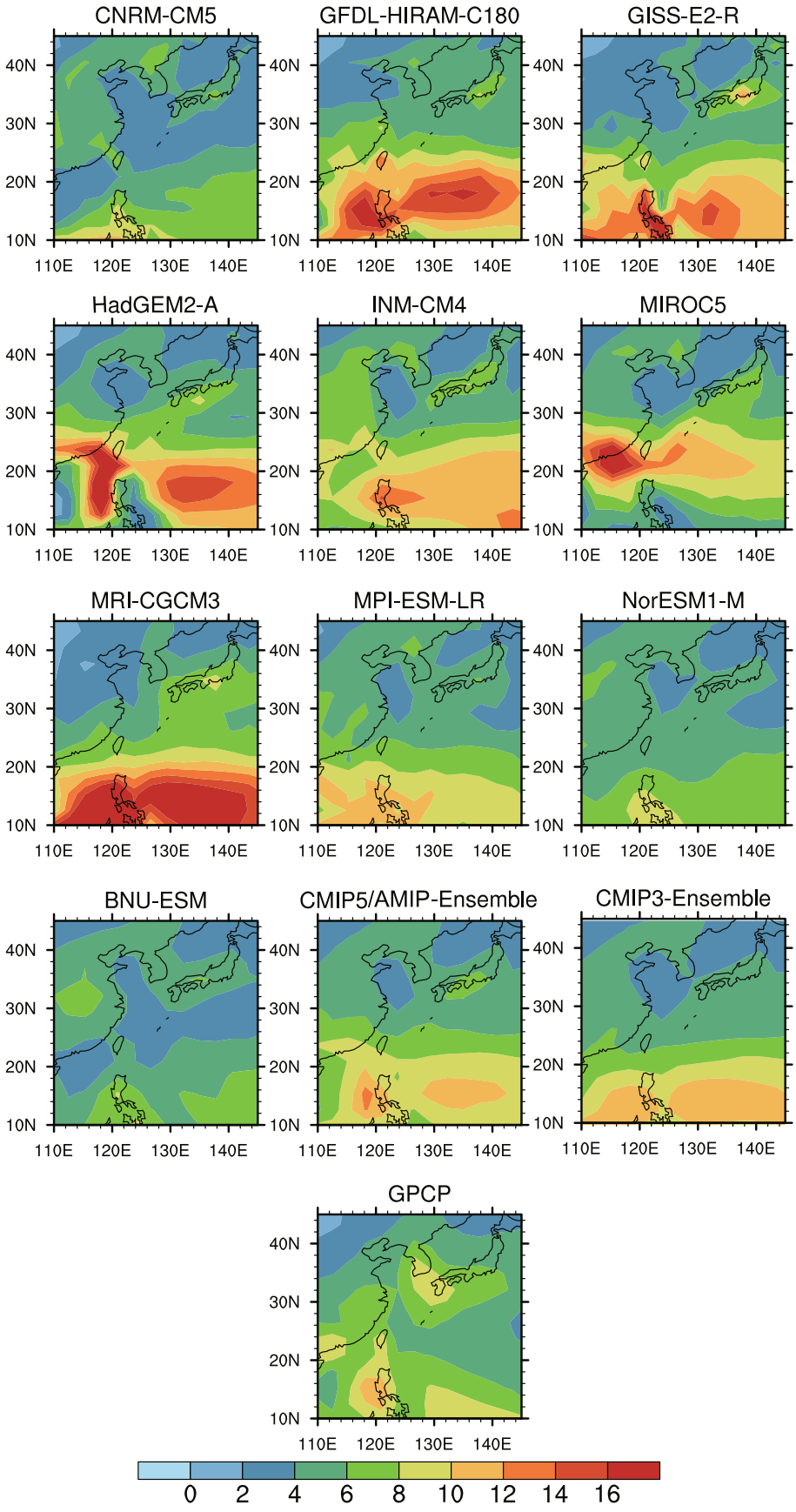

Fig. 1. Observed and simulated climatic JJA (June–August) precipitation (mm d^{-1}) over East Asia during 1979–2008.

nearly all the models (including the CMIP5/AMIP MME) underestimate the precipitation over the Meiyu/Changma/Baiyu front, especially over the East China Sea. Generally, compared with the simulation of the AMIPII MME, the CMIP5/AMIP models improve the representation of tropical and subtropical rainfall slightly.

A Taylor diagram is produced to evaluate the models' integrated performance in simulating the rainfall distributions over EA. In a Taylor diagram, the observed field is represented by a point (identified as "REF") at unit distance from the origin on the horizontal axis. The standard deviation of the modeled field is the radial distance from the origin. The centered root-mean-square error (RMSE), used to quantify the pattern biases between simulation and observation, is the distance to the observed point. The azimuthal position gives the spatial correlation coefficient between the observed and corresponding simulated fields. Note that the centered RMSE and the modeled standard deviation have been normalized by the observed standard deviation.

It is clear that all the models are relatively skillful in reproducing the general patterns of precipitation over EA (Fig. 2). However, some models perform poorly in depicting the amplitude of the variation of precipitation, as might be expected from the constraints of the AMIP experiments (AMIP experiments lack the coupling of atmosphere and ocean). GISS-E2-R and the CMIP5/AMIP MME show relatively higher skill in simulating precipitation over EA than the other models. Furthermore, the CMIP5/AMIP models show better simulation skill than the AMIP II models on the whole.

Generally, the RMSE between simulations and observation can be resolved into two components: differences in the overall means and errors in the patterns of variation. Taylor diagrams do not provide information about overall biases, as the means of the fields are subtracted out before computing their second-order statistics (Taylor, 2001). Thus, the RMSE of the original field is then adopted to measure the differences in mean states between simulated and observed fields. Table 2 shows that the MME can be considered to provide the better simulation of rainfall over EA than any single model The CMIP5/AMIP MME has lower RMSE compared with that of the AMIP II models.

3.2. *Monsoon circulation*

The precipitable water over EA in summer comes from three dominant monsoon streams at low altitude according to observation (Fig. 3). They are: (1) strong southwesterly wind from the Indian summer monsoon; (2) West Pacific southwesterly wind; and (3) cross-equatorial winds from 105° to 150°E. In the simulations of all the CMIP5/AMIP models, the southerly component of the cross-equatorial winds are weaker than that in observation, which leads to the inadequate rainfall over East China. Additionally, negative biases of West Pacific southeasterly wind, which exist in all the models, bring about the less precipitation over the Meiyu/Changma/Baiyu front. The BNU-ESM, CNRM-CM5 and NorESM1-M models simulate weaker southwesterlies over the Bay of Bengal and a resulting drier South China. The air stream extents to the West Pacific are stronger when simulated by GFDL-HIRAM-C180, GISS-E2-R, HadGEM2-A, MIROC5 and MRI-CGCM3. The biases give rise to much precipitation over South China in these five models. The different configurations of the Tibetan Plateau due to the different spatial resolutions of each model (Table 1) may be one of the key dynamic and thermodynamic reasons leading

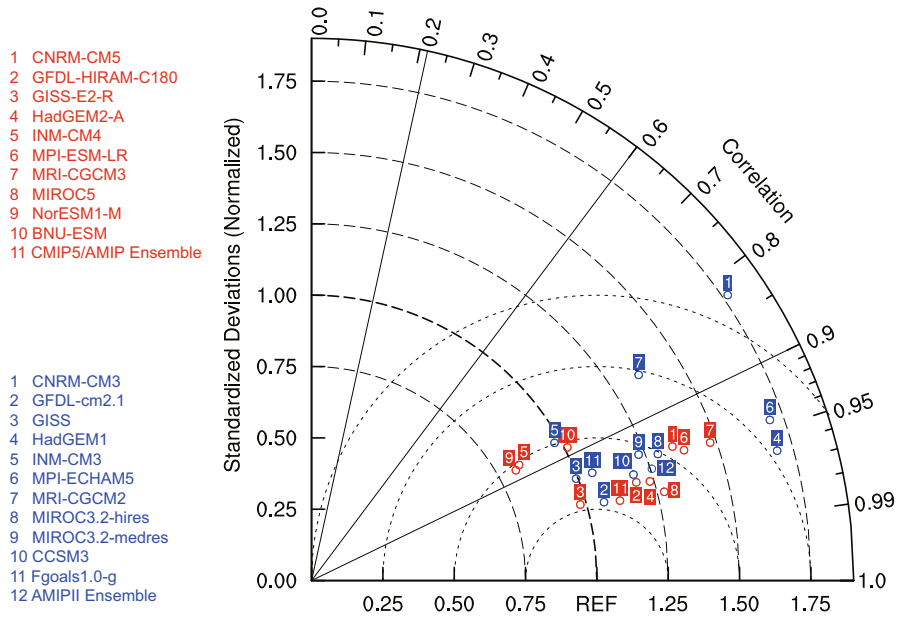

Fig. 2. Taylor diagram of simulated climatic JJA (June–August) precipitation over East Asian from CMIP5 models (red) and AMIP II models (blue).

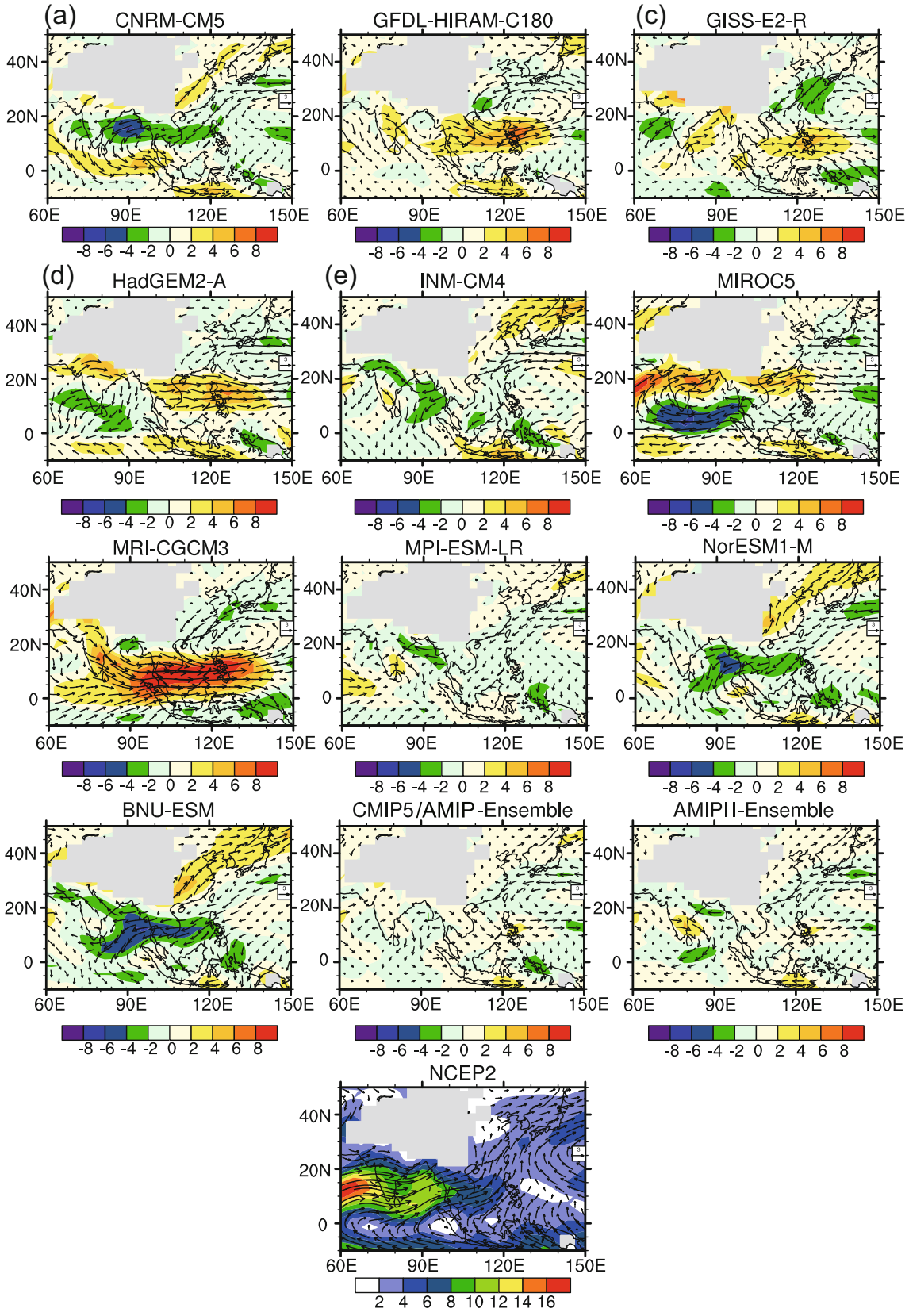

Fig. 3. Differences of simulated and observed (NCEP2) climatic JJA (June–August) horizontal wind fields (vector, units: m s^{-1}) and wind speed (colored shading, units: m s^{-1}) at 850 hPa over East Asia during 1979–2008. But the last panel represents the original observation from NCEP2 data.

to the different biases of air streams at low levels. Compared to each model, the simulated southwesterly, cross-equatorial and southeasterly winds are all improved in the CMIP5/AMIP MME, which is similar with the result of the AMIP II MME, and is then next best in MPI-ESM-LR and INM-CM4. The RMSE of wind speed and direction between simulations and observation over the target region (10°S–50°N, 60°–150°E) is calculated (Table 2) to objectively analyze the simulation of the monsoon air stream. MPI-ESM-LR and the CMIP5/AMIP MME, which is superior to the AMIP II MME, show better skill in simulating the wind field at 850 hPa.

At the upper level, the subtropical westerly jet stream plays an essential role in dynamical aspects of EASM. The location and intensity of the jet stream is closely related with the Meiyu/Changma/Baiyu fronts (Tao et al., 1958; Liang and Wang, 1998; Lau et al., 2000). As shown in Fig 4, the main body of the westerly jet, which is located around 40°N with the jet core (zonal winds greater than 30 m s^{-1}) at 90°E in observations, is farther poleward in most CMIP5/AMIP model simulations, and similar in the simulations of the AMIP II models (Liang et al., 2001; Wang et al., 2011; Wang et al., 2013). The intensity of the westerly jet is weaker in most of the models compared with observation. This gives rise to anomalous easterlies over 20°–40°N and then weakened divergence of the South Asia High, coupled with weakened convergence of air streams over low altitudes. These in turn lead to drier conditions over the region extending from the Yangtze River valley to southern Japan and wetter conditions in southern China. The RMSE of zonal wind speed on 200 hPa between simulations and observation over (35°S–45°N, 110°–150°E) is calculated (Table 2) to objectively analyze the simulation of the westerly jet. As can be seen, model biases of the westerly jet stream are least in the simulations by MRI-CGCM3 and MPI-ESM. However, the AMIP II MME shows lower RMSE than the CMIP5/AMIP MME.

In the middle and lower troposphere, the pattern, position and strength of the WPSH greatly influence EASM precipitation. Three indices are used to comprehensively compare between simulations and observation, i.e., the intensity (I_s), northern edge (I_n) and westward extension (I_w) of the WPSH (Chen et al., 2010). I_s is defined as the regional average of the grids with geopotential height (GHT) greater than 5860 gpm over the region (10°–40°N, 100°–140°E). Note that, if the GHT of all grids over the target region is less than 5860 gpm, the regional averaged GHT is considered as I_s for quantitative comparison. For the definition of I_w, each grid of 500-hPa GHT over the region is firstly subtracted by I_s to obtain a difference field, and then the longitude of the most western boundary of the zero contour of this field is denoted as I_w. The latitude of the WPSH ridge position is defined as I_n, where $u = 0$ and $\partial u/\partial y > 0$ are required (Li and Chou, 1998).

As shown in Fig. 5, the models fall into two distinct groups on the basis of the spatial pattern of the WPSH. In the simulations of group I (GFDL-HIRAM-C180, GISS-E2-R, HadGEM2-A, INM-CM4, MRI-CGCM3 etc.), the WPSH moves to a location east of that observed, with small meridional span and strength. However, the WPSH in group II models (BNU-ESM, CNRM-CM5, MPI-ESM-LR, MIROC5, NorESM1-M etc.) is stronger and extends markedly to the west compared to observation. The averaged biases of I_s, I_w and I_n were computed to provide an integrated score of the WPSH simulations (Table 2). MPI-ESM-LR, MIROC5, NorESM1-M and the CMIP5/AMIP MME also show better skill in their WPSH simulations. Although the AMIP II MME simulates more actual intensity and westward extension of the WPSH, the large biases of the northern edge reduce its entire skill. Although the weak rainfall is obvious in all of the models, the reasons for it are different in the two model groups. The weak and eastward WPSH in group I models leads to less water vapor being transported to the

Table 2. Integrated features by observations and simulations.

Model	UV850			U200	WPSH				Pr CPC				WNPMI
	Precip RMSE	Speed RMSE	Angle RMSE	Speed RMSE	I_s	I_w	I_n	Bias	PC1		PC2		CC
	(mm d^{-1})	(m s^{-1})	(degree)	(m s^{-1})	(hPa)	(lon)	(lat)	(%)	CC	Var.	CC	Var.	
OBS	0.0	0.0	0.0	0.0	5871.2	120	24.3	0.0	1.0	12.18	1.0	6.19	1.0
CNRM-CM5	2.37	1.88	55.00	6.13	5874.3	108	26.2	6.0	0.14	15.89	−0.54	8.97	0.47
GFDL-E2-R	3.93	1.86	46.72	3.32	5861.8	135	20.9	8.8	0.27	13.83	0.06	6.63	0.45
GISS-E2-R	3.17	1.73	39.93	4.48	5797.4	NAN	21.4	NAN	0.50	7.94	−0.17	8.82	0.44
HadGEM-A	4.11	2.05	49.74	7.83	5837.5	145	19.3	14.0	0.36	11.50	0.28	11.97	0.49
INM-CM4	2.95	1.77	80.63	9.38	5828.2	147	24.7	8.2	0.28	8.73	0.06	7.68	0.69
MIROC5	3.54	2.46	42.42	8.74	5868.6	115	25.8	3.4	0.35	12.08	0.11	20.10	0.50
MRI-CGCM3	5.07	3.40	48.81	1.84	5862.3	135	16.4	15.1	0.20	5.59	0.30	8.54	0.55
MPI-ESM-LR	1.82	1.17	28.35	2.06	5870.2	121	24.2	0.5	0.38	15.86	−0.05	10.20	0.49
NorESM1-M	1.89	1.79	60.86	7.13	5878.3	114	26.2	4.4	0.08	14.41	0.29	7.77	0.17
BNU-ESM	2.23	2.13	73.52	4.52	5880.4	110	26.3	5.6	0.09	18.91	0.12	9.79	0.46
CMIP5/AMIP MME	1.98	1.06	26.72	4.12	5863.0	132	23.4	4.7	0.45	13.17	−0.03	11.26	0.73
AMIP II MME	2.28	1.16	29.00	3.62	5867.6	115	18.6	9.2					0.77

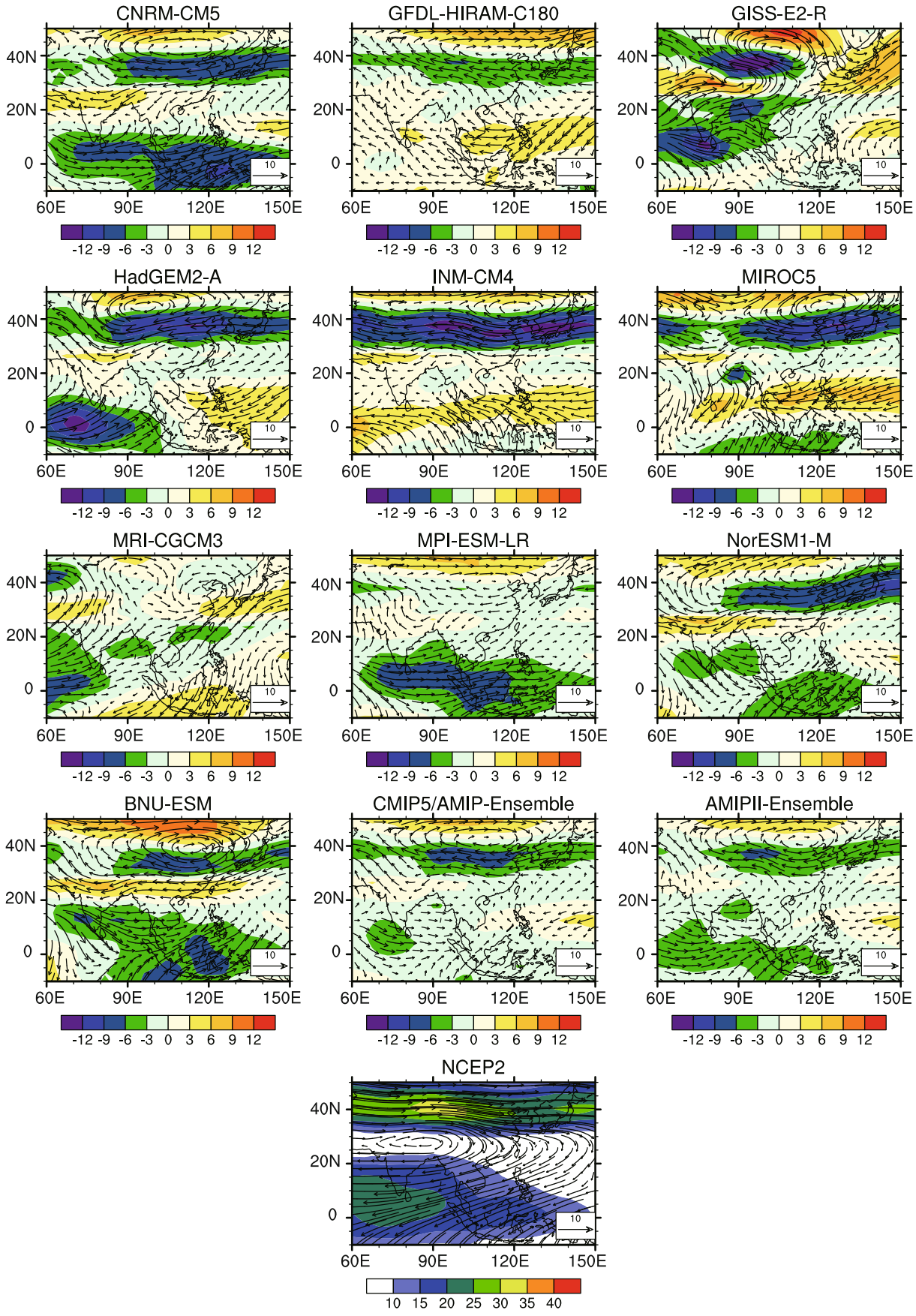

Fig. 4. The same as Fig. 3 but for wind at 200 hPa.

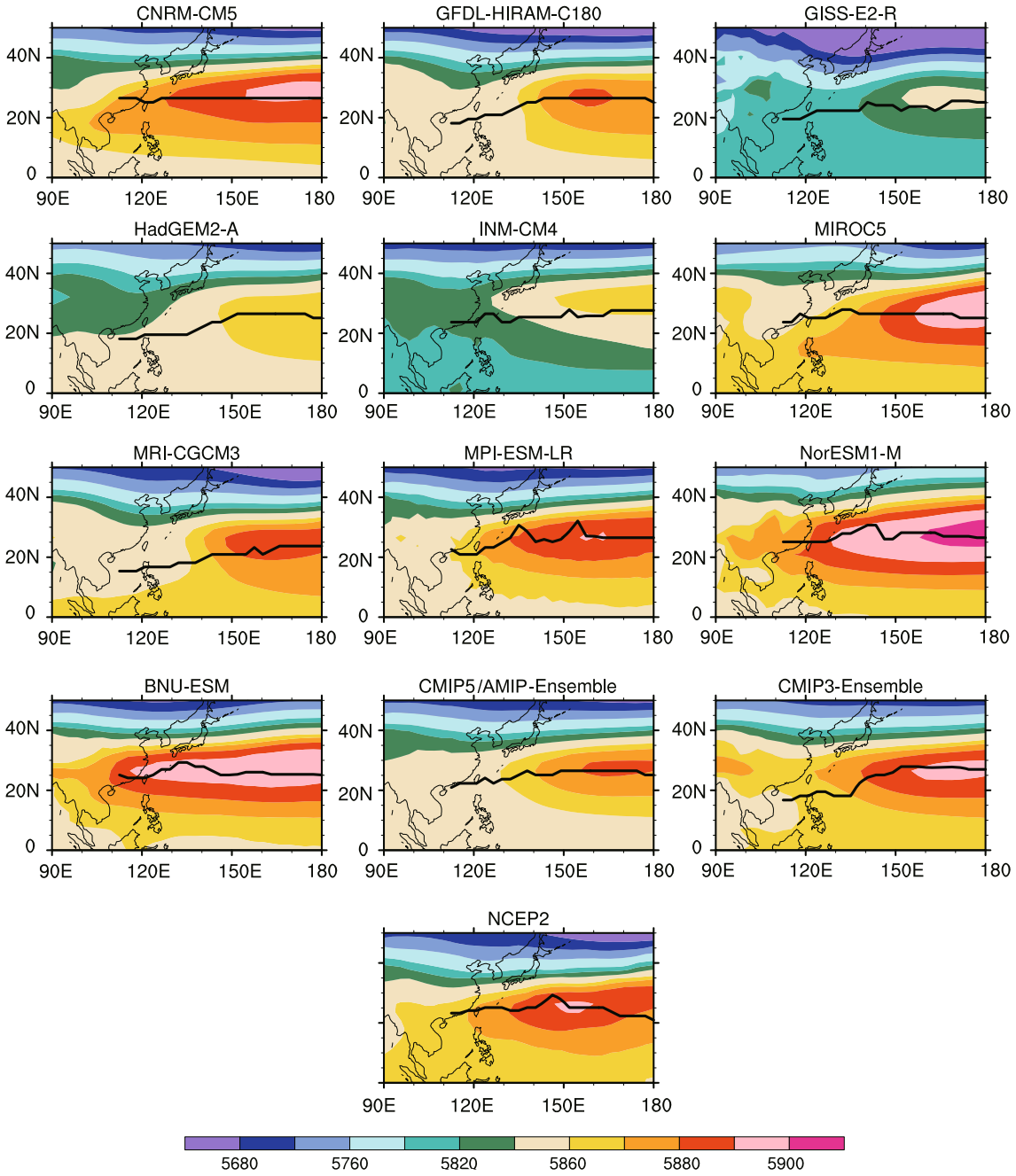

Fig. 5. Observed and simulated climatic JJA (June–August) 500-hPa geopotential height (shading, units: gpm) and WPSH ridge line (black line) over East Asia during 1979–2008.

Meiyu/Changma/Baiyu front; while the strong and westward WPSH in group II models brings less precipitation because the front is controlled by the subtropical high. As a result, the simulation of the Meiyu/Changma/Baiyu rainbelt is largely modulated by the WPSH. Moreover, the WPSH is modulated by the available potential energy generated by the differential heating between land and sea (Li and Yanai, 1996; Zhang et al., 1997). In the AMIP experiment, uniform observed SST is used by each model. Furthermore, tropical latent heat and plateau sensible heating are the main thermal sources in EA. Therefore, the systematic biases of the WPSH in the models should be linked to the biases in heating sources. Hence, the dynamical response to the Plateau's warming, especially in the downstream region, and reasonable simulation of tropical circulation, are required to obtain more realistic simulation of the EASM.

4. Seasonal evolution of EASM

Seasonal evolution is a typical characteristic of EASM (Ding, 2007). To conveniently describe the precipitation center, we define the largest precipitation axis (LPA) as

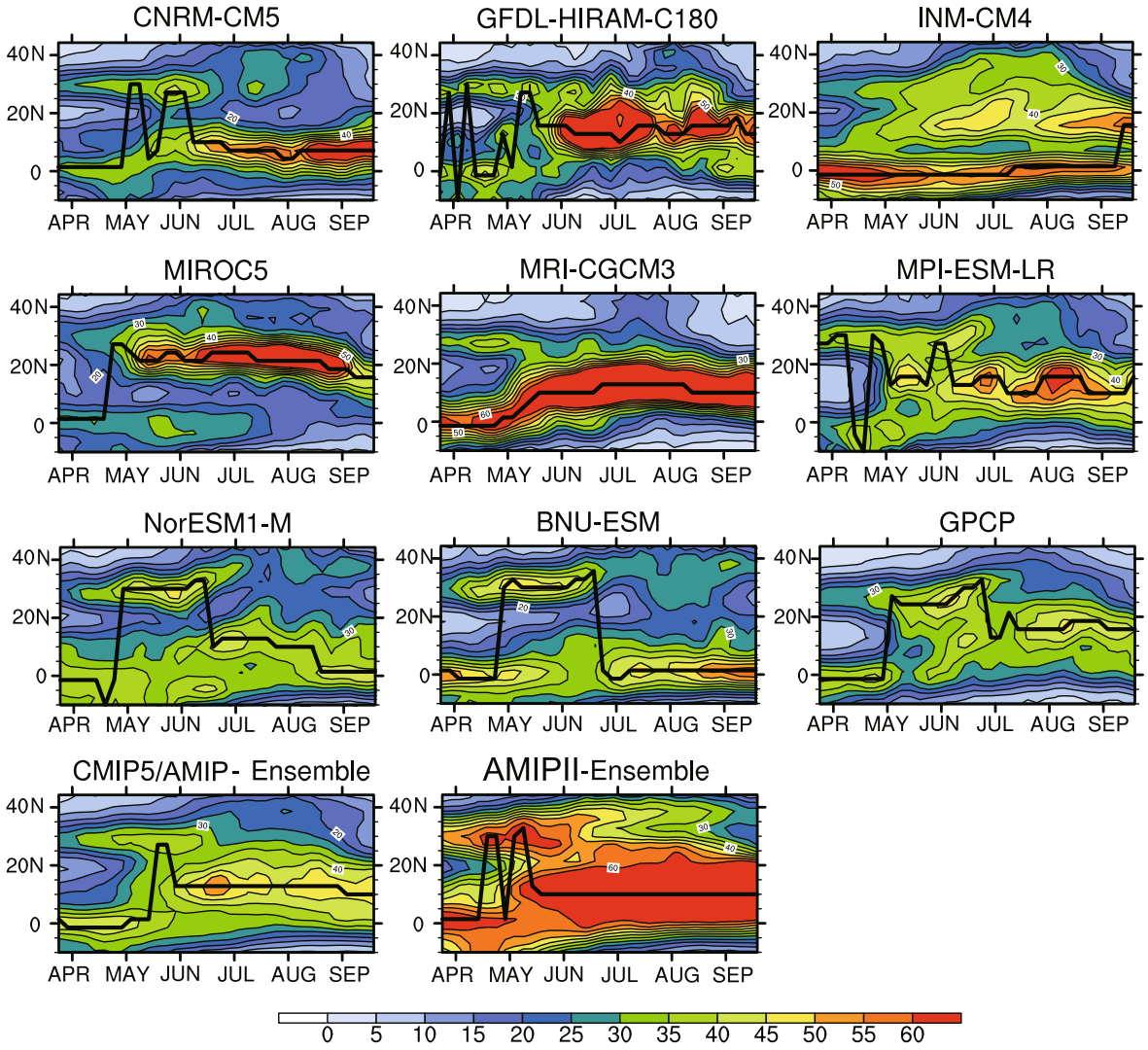

Fig. 6. Observed and simulated climatic seasonal migration of the monsoon rainband zonallyaveraged between 110°E and 120°E and the largest precipitation axis (LPA) during 1979–2008. The pentad data for the observation and 5-day averages from daily data for the model simulations are used.

the meridional (110°–120°E) rainfall maximum in EA between 10°S and 45°N. The seasonal evolution of monsoon precipitation over 110°–120°E and the LPA are shown in Fig. 6.

The LPA indicates that the monsoon rainbelt experiences three northward jumps during boreal summer. In the period before mid-May, southern China experiences a pre-monsoon rainy season and after that the onset of EASM takes place at 20°–30°N accompanied by increased precipitation. In mid-June, the monsoon rainbelt reaches the Yangtze River valley which then experiences the Meiyu/Changma/Baiyu rainy season. In early July, the monsoon rainbelt makes a jump toward northern China and remains there for about one month. From the end of August to early September, it then rapidly retreats to southern China, marking the end of the EASM period. As can be seen from Fig. 5, all of the models capture the broad migration of the rainfall albeit with many systematic errors (note that daily rainfall is not provided by GISS-E2-R, and it is not convenient to handle in the HadGEM2-A model; thus, the results of these two models are not shown). Compared with observation, all of the models except for GFDL-HIRAM-C180 and INM-CM4 are also able to capture the onset of EASM from prior to mid-May. However, other migration features of the rainbelt are not well simulated except for in the BNU-ESM and NorESM1-M models. These two models capture the notable jumps of the LPA and the persistence of the rainbelt over EA. However, the retreat of the rainbelt is exaggerated, moving farther south of that observed. Moreover, an abnormal dry tongue in some simulations located near 20°N from April to July can be seen. The CMIP5/AMIP MME improves the retreat of the rainbelt and the occurrence of this dry tongue, but large biases of notable northward jump and persistence still exist. However, compared with the AMIP II MME, the CMIP5/AMIP MME simulates a more reasonable strength of rainfall as well as the time when the northward jump occurs.

5. Interannual variation of EASM

5.1. *Modes of variability of precipitation over EA*

Empirical orthogonal function (EOF) decomposition is a method aimed at single variable fields with spatiotemporal distribution. For several variable fields to be compared, if each variable field is decomposed by the EOF method, and then their eigenvectors and time series respectively compared, it is very difficult to obtain objective results due to the original field being decided by the eigenvector and time-coefficient combined. Therefore, we used the common EOFs method to analyse the interannual variability of EA precipitation for all simulated and observed data. The common EOFs analysis deals with a direct comparison of the data from all the models and observation on a set of common eigenvectors. The time series from simulation and observational data represent exactly the same spatial pattern. The common EOFs method had been applied previously in analyses and comparisons among AOGCMs (Barnett, 1999; Benestad, 2001).

The principle of the common EOFs method is that two or more data fields with data points on a common grid are concatenated along the time axis, and an EOF analysis is applied to the combined dataset. The detail of the technique is as follows:

For k variable fields $X_i(s,\eta), i = 1,2,\cdots,k$, where s denotes spatial points, suppose time length is T, then $\eta = 1,2,\cdots,T$, to construct a combined variable field $X(s,t), t = 1,2,\cdots,kT$ as follows:

$$X(s,t) = \begin{cases} X_1(s,\eta), \eta = 1,2,\cdots,T; & t = 1,2,\cdots,T \\ X_2(s,\eta), \eta = 1,2,\cdots,T; & t = T+1,T+2,\cdots,2T \\ \vdots & \vdots \\ X_k(s,\eta), \eta = 1,2,\cdots,T; & t = (k-1)T+1,(k-1)T+2,\cdots,kT \end{cases}$$

Apply EOF to X, and get time series of length kT, common eigenvector $\boldsymbol{V}$, and eigenvalue Λ. According to V and the original field X_i, we can also obtain the time series $T_i = V'X_i$.

The eigenvalue Λ cannot reflect the explained variance of the principal component of every variable field. From the meaning of the variance explained by the eigenvalue, we define the ith variable field's eigenvalue $\Lambda_i : \Lambda_i = diag(C_i), C_i = T_i T_i'$.

Now T_i is not strictly orthogonal, but the elements outside the diagonal of the covariance matrix C_i are relatively small, so T_i is close to orthogonal, and there is weak pertinence between different components.

Here, we use simulated and observed precipitation in JJA during 1979–2008 to perform common EOFs analysis. The domain (0°–50°N, 100°–140°E) which includes the closely related tropical northwest Pacific and subtropical East Asian regions is chosen. The results indicate that the models present a basic common pattern but there is strong variation in the amplitude of the corresponding modes. As shown

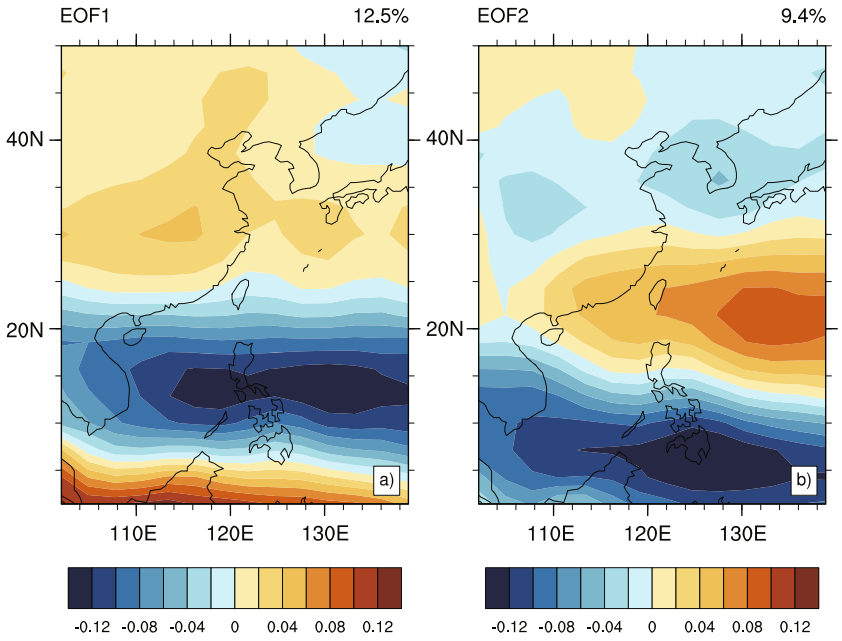

Fig. 7. The leading and second common principal component (CPC) of the East Asian summer (JJA) precipitation by each model, the MME and GPCP data. The data in the top right corner are the common explained variances of the eigenvectors.

in Fig. 7a, the spatial distribution of the first mode shows a north–south dipole with decreased (or increased) precipitation over the northern South China Sea and Philippine Sea and increased (or decreased) precipitation extending from the Yangtze River valley to the south of Japan, covering the Meiyu/Changma/Baiyu front. The spatial distribution of the second mode shows a tripole with wet (or dry) anomalies over the area of 20°–30°N, dry (or wet) anomalies covering the south of the South China Sea to the West Pacific, and wet (or dry) anomalies north of 30°N. The variances of the leading modes are small because of the scattered pattern of rainfall.

Although the models present a basic common pattern there is strong variation in the amplitude of the corresponding modes. The observed time evolution of the leading mode (PC1) shown in Fig. 8a indicates an obvious quasi-biennial oscillation of summer rainfall over EA, consistent with the frequency of drought and flood disasters in the Yangtze River and the Huaihe River valleys (Huang et al., 2007). This is a significant characteristic of the interannual variability of EASM. The major peaks (1980, 1983, 1988, 1998 and 2003) in the observation primarily occur in the summers following the mature phases of El Niño events with above-normal rainfall over the Yangtze River Basin. Under these conditions, a weak summer monsoon may be expected (National Climate Center of China, 1998). The mechanisms responsible for this "prolonged" impact of ENSO or a "delayed" response of the EASM to ENSO is characterized by positive feedback between the off equatorial moist atmospheric Rossby waves and the underlying SST anomaly in the local monsoon warm pool region. Thus, even though the SSTA disappears during the summer after the peak El Niño, the EASM remains to be significantly affected by the northwest Pacific Ocean subtropical anomalies as shown by the leading mode of the EASM (Wang et al., 2000).

The observed temporal evolution of the second mode (PC2; Fig. 8b) shows a large decadal component with a sharp change in 1990–91 (Wang et al., 2008). The observed major peaks occur in El Niño developing years (1982, 1985, 1990, 1994, 1997, 2002, and 2004) and the observed minima of PC2 (1980, 1983, 1991, 1995, 2000) occur in La Niña conditions. Thus, the second mode is primarily associated with developing El Niño and La Niña events (Liu et al., 2008). However, a notable interdecadal change of the EASM–ENSO relation occurred around the late 1970s and 1990s modulated by the climate shifts (Wu and Wang, 2002; Yim et al., 2008; Wang et al., 2011; Ye and Lu, 2011). Before the 1977/78 climate shift and after the 1992/93 climate shift, Meiyu rainfall levels are above normal in most La Niña years; whereas during the period 1979–91, Meiyu rainfall is usually below normal levels in La Niña years (Wang et al., 2012).

As shown in Figs. 8a and 8b, each model produces various amplitudes of interannual variability of rainfall. Correlation coefficients and variance are used to investigate the simulation of leading PCs. Table 2 shows that the two PCs simulated by most models have little similarity with those in observations. For PC1, the ensemble of models has the largest similarity with observation. For PC2, which is primarily associated with developing ENSO events and has a large

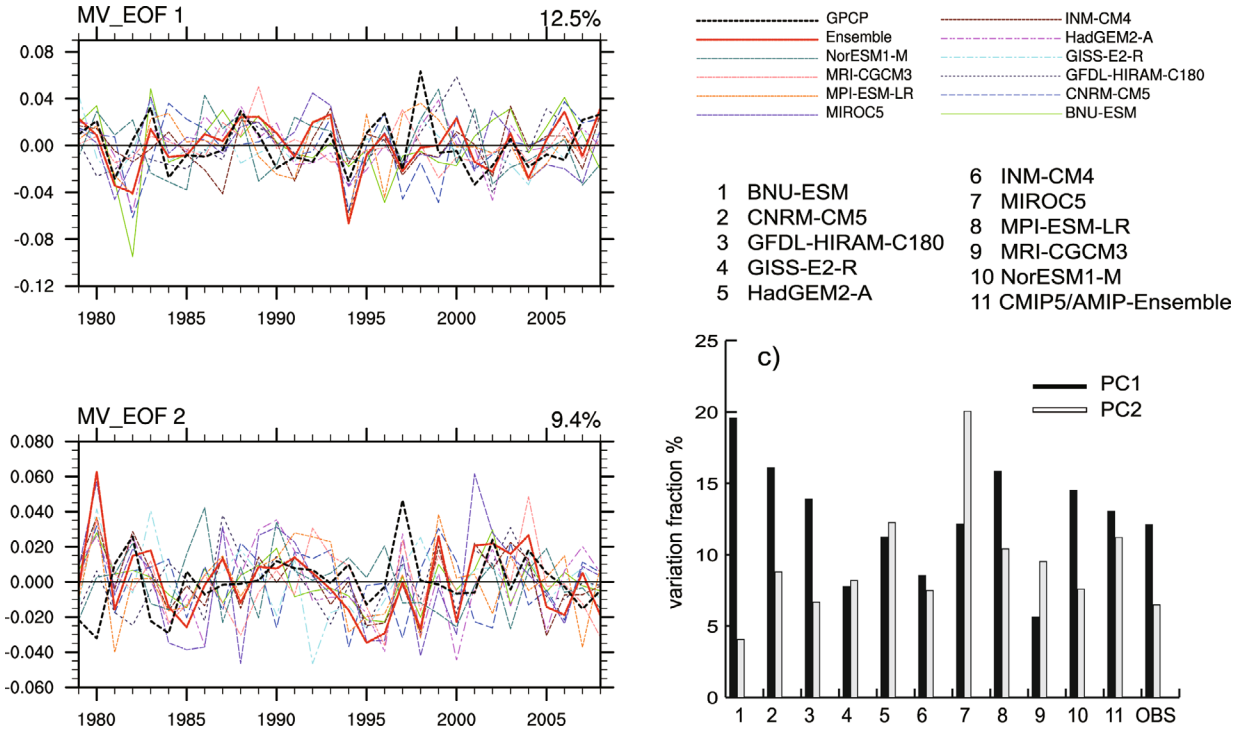

Fig. 8. Time series of the principal components (PCs) of the (a) first and (b) second modes in Fig. 6. Panel (c) is a bar chart showing the percent variance explained by the leading two CPCs for precipitation for each model and for observations.

decadal component, except for MRI-CGCE3 and NorESM1-M, the skill of other models is poor. Thus, most of the models fail to capture the interannual variation corresponding to the second mode of the rainfall over EA.

The leading and second modes account for about 12.5% and 9.4% of the total variance in entire series of all simulations and observation. By further investigating the explained variances of PCs of each model to the common EOFs pattern (Fig. 8c), we find the leading and second modes account for about 12.2% and 6.2% of the variance in the observation, and about 13.2% and 11.3% in MME result. However, GISS-E2-R, HadGEM2-A, MIROC5 and MRI-CGCM3, whose RMSEs of climatic rainfall over EA are large, simulate larger variances of the second mode than that of the leading mode. Among all the CMIP5/AMIP models, NorESM1-M simulates the most similar explained variances to observation.

5.2. *Interannual variation of EASM circulation*

EASM circulation parameters, instead of rainfall, are always used to depict the interannual variation of EASM, partly because of the complex rainfall structure and partly due to a preference of using large-scale winds to define the broad-scale monsoon. To quantify the variability of EASM circulation, the meridional differences of the 850-hPa zonal winds (U_{850}) are used to define the circulation indices (Wang and Fan, 1999); that is

$$\mathrm{WNPMI} = U_{850}(5^\circ\text{–}15^\circ\mathrm{N}, 100^\circ\text{–}130^\circ\mathrm{E}) - U_{850}(20^\circ\text{–}30^\circ\mathrm{N}, 110^\circ\text{–}140^\circ\mathrm{E}) ,$$

where the regions in parentheses denote the regions over which U_{850} is averaged. The traditional Chinese meaning of a strong EASM (high index) corresponds to a deficient Meiyu associating with its abnormal northward extension of southerly winds over northern China.

The temporal series of WNPMI from 1979 to 2008 (the AMIP II MME is from 1979 to 1999) are shown in Fig 9. The interannual variation is obvious in each model with various phases and amplitudes. Table 2 shows that although correlation coefficients between most models and observation pass the 99% significant test, half of them overestimate the amplitude of EASM variation, which produces the large variance of precipitation. The CMIP5/AMIP MME is skillful in its simulation of WNPMI for its large correlation coefficient and the WNPMI power spectrum (Fig 10) shows that there are two dominant peaks in the observation—a quasi-biennial period and a quasi-quadrennial period. These two cycles are apparent in GFDL-HIRAM-C180, INM-CM4, NorESM1-M and the CMIP5/AMIP MME.

6. Summary and Conclusions

To understand the skill of AGCMs in capturing major features of EASM, 10 models that participated in the CMIP5/AMIP, which used observational SST to drive the AGCMs for the period 1979–2008, are evaluated by comparing with observations. The results provided a clear conclusion that the CMIP5/AMIP MME has the best skill in terms of simulating EASM better in general than the AMIP II MME. In addition, it is found that different models show varying abilities in each aspect of EASM simulations. The main findings are as follows:

Generally, compared with the AMIPII MME, the CMIP5/AMIP MME shows improved simulation of EASM. The CMIP5/AMIP MME captures most part of the realistic features of precipitation, winds and geopotential height. Furthermore, it is found that the simulations of the Meiyu/Changma/Baiyu rainbelt are largely modulated by the WPSH. In group I models (GFDL-HIRAM-C180, GISS-E2-R, HadGEM2-A, INM-CM4, MRI-CGCM3 etc.), the Meiyu/Changma/Baiyu front is weakly simulated by a weak WPSH and accompanying eastward southwesterly winds. Meanwhile, in the simulations of group II models (BNU-ESM, CNRM-CM5, MIROC5, MPI-ESM-LR, NorESM1-M etc.),

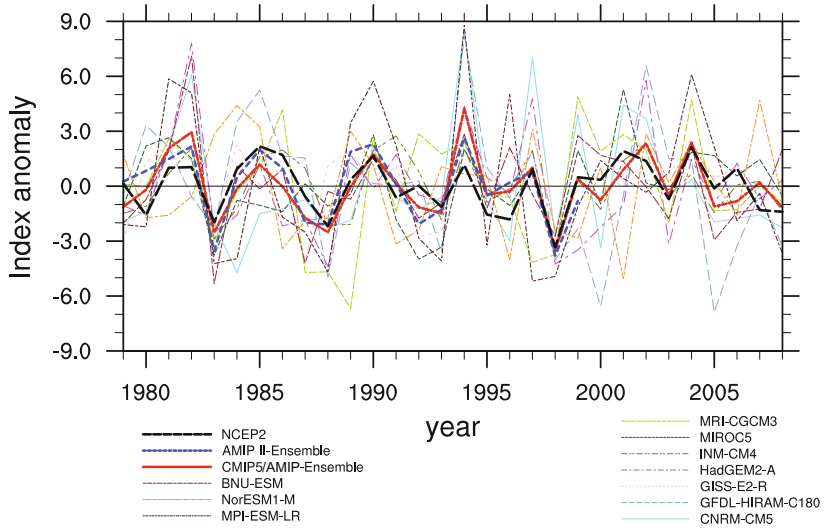

Fig. 9. Observed and simulated WNPMI from 1979 to 2008.

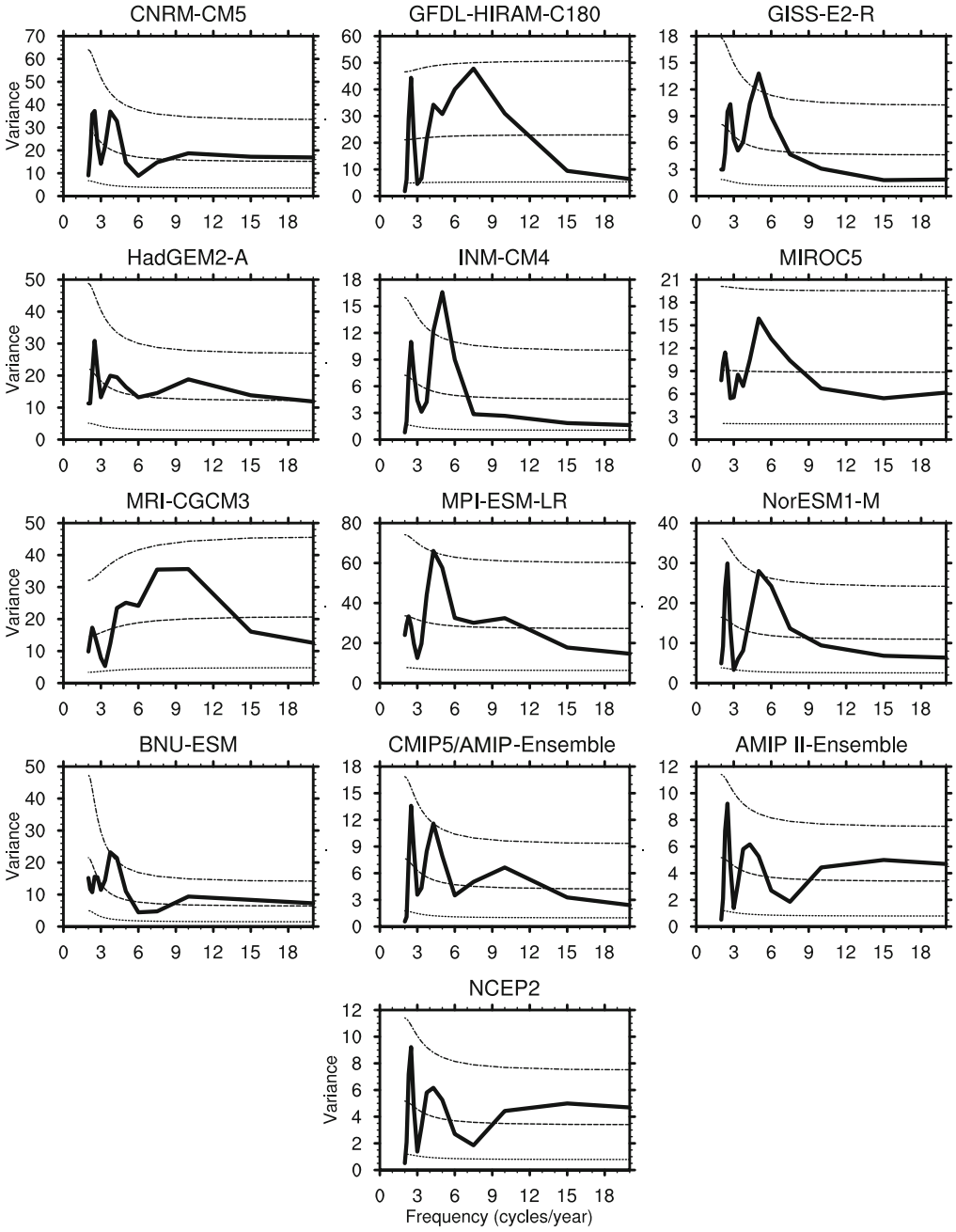

Fig. 10. Observed and simulated WNPMI power spectra. In each plot, the dotted lines from top to bottom are upper confidence bound (95%) for Markov, red noise spectrum and lower confidence bound (5%) for Markov. The heavy lines indicate the WNPMI power spectra.

the weak fronts are caused by a too strong and west-extended WPSH. Moreover, the subtropical upper westerly jet stream plays an essential role in dynamical aspects of EASM. The location and intensity of the jet stream is closely related with the Meiyu/Changma/Baiyu fronts. WPSH is closely related to the large-scale land-sea thermal contrasts. The systematic biases of the WPSH in the models should be linked to the biases in heating sources. Hence, the dynamical response to the Plateau's warming, especially in the downstream region, and reasonable simulation of tropical circulation, are required to obtain more realistic simulation of the EASM.

The prominent features of seasonal migration can be captured by most of the CMIP5/AMIP models, but considerable systematic errors exist. Most of the models cannot capture the notable jumps and persistence of the subtropical rainbelt. The CMIP5/AMIP MME improves the retreat of rainbelt and presence of a dry tongue but large bias also exists.

The results of common EOF analysis of the rainfall over EA show that ensemble of models has the most similarity with observations for PC1. But the skill of all models except

for MRI-CGCE3 and NorESM1-M is poor for PC2, which is primarily associated with developing ENSO events and has a large decadal component. Among all the CMIP5/AMIP models, NorESM1-M simulates the most similar explained variances to observations.

The CMIP5/AMIP MME is skillful in terms of simulating WNPMI for its large correlation coefficient. Additionally, two dominant peaks in observations—a quasi-biennial period and a quasi-quadrennial period—are apparent in the simulations of GFDL-HIRAM-C180, INM-CM4, NorESM1-M and the CMIP5/AMIP MME.

Acknowledgements. This study was supported by the National High Technology Research and Development Program of China (Grant No. 2010AA012305), the General Project of the National Natural Science Foundation of China (Grant No. 41275108), the National Basic Research Program of China (Grant No. 2010CB950504) and the Fundamental Research Funds for the Central Universities (Grant No. 2012YBXS27).

REFERENCES

Adler, R. F., and Coauthors, 2003: The version-2 global precipitation climatology project (GPCP) monthly precipitation analysis (1979–present). *J. Hydrometeorology*, **4**(6), 1147–1167.

Barnett, T. P., 1999: Comparison of near-surface air temperature variability in 11 coupled global climate models. *J. Climate*, **12**, 511–518.

Benestad, R. E., 2001: A comparison between two empirical downscaling strategies. *Inter*. J. *Climatol*., **21**, 1645–1668.

Bentsen, M., and Coauthors, 2012: The Norwegian Earth System Model, NorESM1-M—Part 1: Description and basic evaluation, *Geosci. Model Dev. Discuss*., 5, 2843–2931, doi: 10.5194/gmdd-5-2843-2012, 2012.

Chen, H. M., T. J. Zhou, R. B. Neale, X. Q. Wu, and G. J. Zhang, 2010: Performance of the new NCAR CAM3. 5 in East Asian summer monsoon simulations: Sensitivity to Modifications of the Convection Scheme. *J. Climate*, **23**, 3657–3675.

Collins, N., and Coauthors, 2008: Evaluation of the HadGEM2 model. Hadley Centre technical note No. 74, 47 pp.

Collins, W. D., and Coauthors, 2006: The community climate system model version 3 (CCSM3). *J. Climate*, **19**(11), 2122–2143.

Ding, Y. H., 2007: The variability of the Asian summer monsoon. *J. Meteor. Soc. Japan*, **85**, 21–54.

Ferranti, L., J. M. Slingo, T. N. Palmer, and B. J. Hoskins, 1997: Relations between interannual and intraseasonal monsoon variability as diagnosed from AMIP integrations. *Quart. J. Roy. Meteor. Soc.*, **123**, 1323–1357.

Gadgil, S., and S. Sajani, 1998: Monsoon precipitation in the AMIP runs. *Climate Dyn.*, **14**, 659–689.

Huang, R. H., J. L. Chen, and G. Huang, 2007: Characteristics and variations of the East Asian monsoon system and its impacts on climate disasters in China. *Adv. Atmos. Sci.*, **24**, 993–1023, doi:10.1007/s00376–007-0993-x.

Kanamitsu, M., W. Ebisuzaki, J. Woollen, S. K. Yang, J. J. Hnilo, M. Fiorino, and G. L. Potter, 2002: Ncep-doe amip-ii reanalysis (r-2). *Bull. Amer. Meteor. Soc.*, **83**, 1631–1644.

Kang, I. S., and Coauthors, 2002: Intercomparison of the climatological variations of Asian summer monsoon precipitation simulated by 10 GCMs. *Climate Dyn.*, **19**, 383–395.

Kim, H.-J., B. Wang, and Q. H. Ding, 2008: The global monsoon variability simulated by CMIP3 coupled climate models. *J. Climate*, **21**, 5271–5294.

Kucharski, F., and Coauthors, 2009: The CLIVAR C20C project: skill of simulating Indian monsoon rainfall on interannual to decadal timescales. Does GHG forcing play a role? *Climate Dyn.*, **33**(5), 615–627.

Lau, K. M., and M. Li, 1984: The monsoon of East Asia and its global associations-A survey. *Bull. Amer. Meteor. Soc.*, **65**(2), 114–125.

Lau, K.-M., K.-M. Kim, and S. Yang, 2000: Dynamical and boundary forcing characteristics of regional components of the Asian summer monsoon. *J. Climate*, **13**, 2461–2482.

Li, C. F., and M. Yanai, 1996: The onset and interannual variability of the Asian summer monsoon in relation to Land-Sea thermal contrast. *J. Climate*, **9**, 358–375.

Li, J. P., and J. F. Chou, 1998: Dynamical analysis on splitting of subtropical high-pressure zone. *Chinese Science Bulletin*, **43**, 1285–1289.

Liang, X.-Z., and W.-C. Wang, 1998: Associations between China monsoon rainfall and tropospheric jets. *Quart. J. Roy. Meteor. Soc.*, **124**, 2597–2623.

Liang, X. Z., A. N. Samel, and W. C. Wang, 1995: Observed and GCM simulated decadal variability of monsoon rainfall in east China. *Climate Dyn.*, **11**(2), 103–114.

Liang, X. Z., W. C. Wang, and A. N. Samel, 2001: Biases in AMIP model simulations of the east China monsoon system. *Climate Dyn.*, **17**, 291–304.

Lin, H., and B. Wang, 2002: The time-space structure of the Asian-pacific summer monsoon: A fast annual cycle view. *J. Climate*, **15**, 2001–2019.

Liu, J., B. Wang, and J. Yang, 2008: Forced and internal modes of variability of the East Asian summer monsoon. *Climate of the Past Discussions*, **4**, 645–666.

Meehl, G. A., and Coauthors, 2006: Monsoon regimes in the CCSM3. *J. Climate*, **19**(11), 2482–2495.

National Climate Center of China, 1998: Heavy flooding and climate anomalies in China in 1998. China Meteorological Press, 139 pp.

Roeckner, E., and Coauthors, 2003: The atmospheric general circulation model ECHAM 5. Part I: Model description. Max-Planck-Institute for Meteorology, Report No. 349, 1–127.

Schmidt, G. A., and Coauthors, 2006: Present-day atmospheric simulations using GISS ModelE: Comparison to in situ, satellite, and reanalysis data. *J. Climate*, **19**, 153–192.

Shukla, J., and M. J. Fennessy, 1994: Simulation and predictability of monsoons. *Proc. the Int. Conf. Monsoon Variability and Prediction*,Tech Rep WCRP-84, WCRP, Geneva, Switzerland, 567-575.

Sperber, K. R., and T. N. Palmer, 1996: Interannual tropical rainfall variability in general circulation model simulations associated with the Atmospheric Model Intercomparison Project. *J. Climate*, **9**, 2727–2750.

Tao, S. Y., Y. J. Zhao, and X. M. Chen, 1958: The relationship between Meiyu in far east and the behaviour of circulation over Asia. *Acta Meteorologica Sinica*, **29**(2), 119–134. (in Chinese)

Taylor, K. E., 2001: Summarizing multiple aspects of model performance in a single diagram. *J. Geophys. Res*., **106**, 7183–7192.

Taylor, K. E., R. J. Stouffer, and G. A. Meehl, 2012: An overview

of CMIP5 and the experiment design. *Bull. Amer. Meteor. Soc.*, **93**, 485–498.

Taylor, K. E., R. J. Stouffer, and G. A. Meehl, cited 2013: A summary of the CMIP5 experiment design (2009). [Available online at http://cmip-pcmdi.llnl.gov/cmip5/experiment_design.html?submenuheader=1]

Voldoire, A., and Coauthors, 2011: The CNRM-CM5.1 global climate model: description and basic evaluation. *Climate Dyn.*, **40**, 2091–2121, doi: 10.1007/s00382–011-1259-y.

Volodin, E. M., N. A. Dianskii, and A. V. Gusev, 2010: Simulating present-day climate with the INMCM 4.0 coupled model of the atmospheric and oceanic general circulations. *Izvestiya, Atmospheric and Oceanic Physics*, **46**, 414–431.

Wang, B., and Z. Fan, 1999: Choice of South Asian summer monsoon indices. *Bull. Amer. Meteor. Soc.*, **80**, 629–638.

Wang, B., and H. Lin, 2002: Rainy seasons of the Asian-Pacific monsoon defined using a single variable. *J Climate*, **15**, 386–398.

Wang, B., R. G. Wu, and X. H. Fu, 2000: Pacific-East Asian teleconnection: How does ENSO affect East Asian climate? *J. Climate*, **13**, 1517–1536.

Wang, B., I. S. Kang, and J. Y. Lee, 2004: Ensemble simulations of Asian-Australian monsoon variability by 11 AGCMs. *J. Climate*, **17**, 803–818.

Wang, B., Q. H. Ding, X. H. Fu, I. S. Kang, K. Jin, J. Shukla, and F. Doblas-Reyes, 2005: Fundamental challenge in simulation and prediction of summer monsoon rainfall. *Geophys. Res. Lett.*, **32**, L15711, doi: 10.1029/2005GL022734.

Wang, B., Z. W. Wu, J. P. Li, J. Liu, C. P. Chang, Y. H. Ding, and G. X. Wu, 2008: How to measure the strength of the East Asian summer monsoon. *J. Climate*, **21**, 4449–4463.

Wang, C. H., X. Z. Liang, and A. N. Samel, 2011: AMIP GCM simulations of precipitation variability over the Yangtze River Valley. *J. Climate*, **24**(8), 2116–2133.

Wang, X., D. X. Wang, W. Zhou, and C. Y. Li, 2012: Interdecadal modulation of the influence of La Niña events on Mei-yu rainfall over the Yangtze River Valley. *Adv. Atmos. Sci.*, **29**(1), 157–168, doi: 10.1007/s00376-011-1021-8.

Wang, X., W. Zhou, D. X. Wang, and C. Z. Wang, 2013: The impacts of the summer Asian Jet Stream biases on surface air temperature in mid-eastern China in IPCC AR4 Models. *Inter. J. Climatol.*, **33**, 265–276, doi:10.1002/joc.3419.

Watanabe, M., and Coauthors, 2010: Improved climate simulation by MIROC5: mean states, variability, and climate sensitivity. *J. Climate*, **23**, 6312–6335.

Webster, P. J., V. O. Maga, T. N. Palmer, J. Shukla, R. A. Tomas, M. Yanai, and T. Yasunari, 1998: Monsoons: processes, predictability, and the prospects for prediction. *J. Geophys. Res.*, **103**(C7), 14 451–14 510.

Wu, Q. Z., J. M. Feng, W. J. Dong, L. N. Wang, D. Y. Ji and H. Q. Cheng, 2013: Introduction of the CMIP5 Experiments Carried out by BNU-ESM. *Advances in Climate Change Research*, **9**(4), 291–294. (in Chinese)

Wu, R. G., and B. Wang, 2002: A contrast of the East Asian summer monsoon-ENSO relationship between 1962–77 and 1978–93. *J. Climate*, **15**, 3266–3279.

Wu, R. G., and B. P. Kirtman, 2007: Observed relationship of spring and summer East Asian rainfall with winter and spring Eurasian snow. *J. Climate*, **20**, 1285–1304.

Ye, H., and R. Y. Lu, 2011: Subseasonal variation in ENSO-related East Asian rainfall anomalies during summer and its role in weakening the relationship between the ENSO and summer rainfall in Eastern China since the late 1970s. *J. Climate*, **24**, 2271–2284.

Yu, Y. Q., R. C. Yu, X. H. Zhang and H. L. Liu, 2004: Global coupled ocean–atmosphere general circulation models in LASG/IAP. *Adv. Atmos. Sci*., **21**, 444–455, doi: 10.1007/BF 02915571.

Yukimoto, S., and Coauthors, 2011: Meteorological Research Institute-Earth System Model Version 1 (MRI-ESM1). Technical Reports of the Meteorological Research Institute No. 64. [Available online at http://www.mri-jma.go.jp/Publish/Technical/ DATA/VOL_64/index_en.html.]

Yim, S. Y., S. W. Yeh, R. G. Wu, and J. G. Jhun, 2008: The influence of ENSO on decadal variations in the relationship between the East Asian and Western North Pacific summer monsoons. *J. Climate*, **21**, 3165–3179.

Zhang, Y., and Coauthors, 1997: East Asian winter monsoon: results from eight AMIP models. *Climate Dyn.*, **13**, 797–820.

Zhao, M., I. M. Held, S. J. Lin and G. A. Vecchi, 2009: Simulations of global hurricane climatology, interannual variability, and response to global warming using a 50 km resolution GCM. *J. Climate*, **22**, 6653–6678.

Zhou, T. J., and J. Zhang, 2011: The vertical structures of atmospheric temperature anomalies associated with two flavors of El Niño simulated by AMIP II models. *J. Climate*, **24**(4), 1053–1070.

Zhou, T. J., B. Wu, and B. Wang, 2009a: How well do atmospheric general circulation models capture the leading modes of the interannual variability of the Asian-Australian monsoon? *J. Climate*, **22**(5), 1159–1173.

Zhou, T., and Coauthors, 2009b: The CLIVAR C20C project: which components of the Asian-Australian monsoon circulation variations are forced and reproducible? *Climate Dyn*., **33**, 1051–1068.